Hydrodynamical assessment of 200A GeV collisions

Ekkard Schnedermann[1] and Ulrich Heinz[2]
[1]*Department of Physics, Brookhaven National Laboratory, Upton, New York 11973*
[2]*Institut für Theoretische Physik, Universität Regensburg, D-93040 Regensburg, Germany*
(Received 8 February 1994)

We are analyzing the hydrodynamics of 200A GeV S+S collisions using a new approach which tries to quantify the uncertainties arising from the specific implementation of the hydrodynamical model. Based on a previous phenomenological analysis we use the global hydrodynamics model to show that the amount of initial flow, or initial energy density, cannot be determined from the hadronic momentum spectra. We additionally find that almost always a sizable transverse flow develops, which causes the system to freeze out, thereby limiting the flow velocity in itself. This freeze-out dominance in turn makes a distinction between a plasma and a hadron resonance gas equation of state very difficult, whereas a pure pion gas can easily be ruled out from present data. To complete the picture we also analyze particle multiplicity data, which suggest that chemical equilibrium is not reached with respect to the strange particles. However, the overpopulation of pions seems to be at most moderate, with a pion chemical potential far away from the Bose divergence.

PACS number(s): 25.75.+r, 47.75.+f

I. INTRODUCTION

The success of hydrodynamics as a model for the space-time evolution of heavy-ion collisions at the Bevelac with center-of-mass energies of several hundred MeV/nucleon [1,2] suggests its basic applicability to the ultrarelativistic heavy-ion collisions at the Brookhaven alternating gradient synchrotron (AGS) with $\sqrt{s} \approx 5\,A$ GeV or at the CERN super proton synchrotron (SPS) with $\sqrt{s} \approx 20\,A$ GeV (e.g., [3–7]). Since the hydrodynamical model [8–11] describes matter during the collision in terms of the collective variables of energy density ε, pressure P, and flow velocity u^μ, its validity should actually improve at higher energies because of the strongly increasing particle multiplicities. Although the model's primary task is the description of the inclusive hadron spectra, which are measured in several experiments at the AGS [12,13] and the SPS [13,14], its reasonably precise picture of the collison dynamics can further on serve as a basic framework for the computation of almost any other observable, e.g., J/ψ, strangeness, $\bar{p}$, dileptons, strangelets, etc.

Moreover, such an effort is also accompanied by the hope that once a reliable hydrodynamical description is achieved we will automatically have information about the yet unknown equation of state of hadronic matter, which serves as the basic input to hydrodynamics. Especially, a first order phase transition from normal hadronic matter to a quark gluon plasma, as suggested by lattice QCD calculations, would result in a coexistence region with $\partial P/\partial\varepsilon \to 0$ and, in principle, might lead to qualitatively new dynamical signatures.

However, we encounter the problem that some of the assumptions underlying the hydrodynamic model may not be sufficiently valid in ultrarelativistic collisions with center-of-mass energies one order of magnitude higher than at the BEVALAC. In particular, the question of whether and when local thermalization can be reached is still under debate, and we do not attempt to answer it in this paper. Instead we will take sufficient thermalization for granted some time after the first hard collisions and only assume validity of the hydrodynamic model thereafter. Apart from thermalization, our approach will differ considerably from previous publications [3–7] in that we will try to resolve the other important uncertainties arising from the specific implementation of hydrodynamics. To achieve this goal we are careful to test each hypothesis when it is introduced, leading to the organization of the paper as follows.

Based on a phenomenological analysis of the hadronic spectra from $S+S$ at 200 A GeV [15], we extract in Sec. II from the measured particle spectra as much information as possible about the hydrodynamical behavior at freeze-out. In Sec. III we use global hydrodynamics as a computationally efficient method [16], to investigate to what extent the initial hydrodynamical state is constrained by the data, and find that the amount of initial longitudinal flow cannot be decided from the data alone. A closer look at two possible extreme scenarios in Sec. IV, namely Landau- and Bjorken-like initial conditions, shows striking similarities in their temperature and transverse flow at freeze-out. In Sec. V we show that the transverse expansion is the most important contributor to the freeze-out process and is thus invariably limited by itself. In Sec. VI we confront our model with the experimental data and note good agreement for a variety of underlying assumptions regarding entropy generation and freeze-out description. Additionally, we test different equations of state and find that only the pure pion gas can be ruled out while the distinction between the plasma and the hadron resonance gas by hydrodynamical means is very hard to accomplish. In Sec. VII we finally address the issue of chemical equilibration and the pion chemical potential by computing particle ratios and multiplicities. Section VIII summarizes our results and conclusions.

II. DATA FROM A HYDRODYNAMICAL POINT OF VIEW

The measured single particle distributions confer basically two distinct types of information: The shape of the measured spectra reflects the temperature and flow dynamics of the system, while the absolute normalization of the spectra is connected additionally with the size of the collision zone and the amount of chemical equilibration among the particle species.

For the moment we will focus exclusively on the shape, leaving the normalization arbitrary until Sec. VII where we return to this issue in detail. Since at SPS energies pions are the overwhelming majority of all produced secondaries, with kaons, nucleons, strange baryons, and antibaryons following in descending order, we will base our analysis preferentially on the pions. This ensures on the experimental side that the spectra can be measured quite accurately with small statistical errors while on the theoretical side the understanding of different effects on the spectra has been developed the furthest. In any case, because the other particles seem to follow the pions (Fig. 2), all species would give very similar results.

As shown in [15], the dynamics of the collision zone shows up in the hadronic spectra, as measured by the NA35 collaboration [17–19], in two distinct ways: The longitudinal flow determines the rapidity distributions, while the transverse flow influences the transverse mass spectra.

The longitudinal flow can be extracted most accurately from the pion rapidity spectrum [4,20,15]. The extracted value is supported by the spectra of all other particles measured by NA35 [17–19]. The rapidity spectra of all

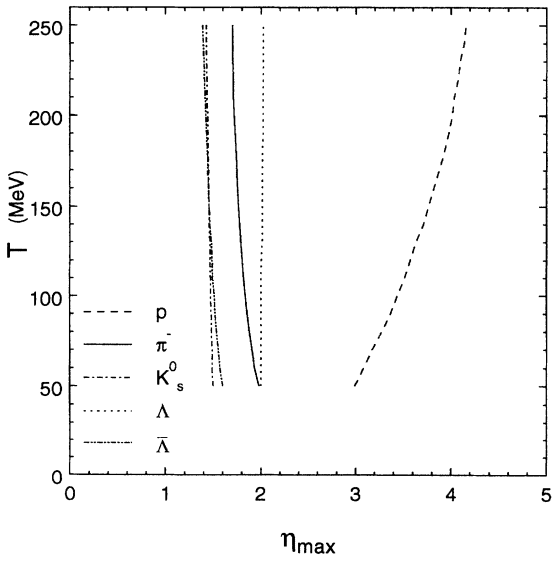

FIG. 1. Every point (T, η_{max}) on these lines corresponds to a fit of the computed y spectra (including resonance decays and longitudinal flow) to the measured ones [17–19]. The longitudinal flow $\eta_{max} \approx 1.7 \pm 0.2$ fits all particle spectra almost independently of the temperature T, with exception of the protons, which still carry a big amount of their initial longitudinal motion [15].

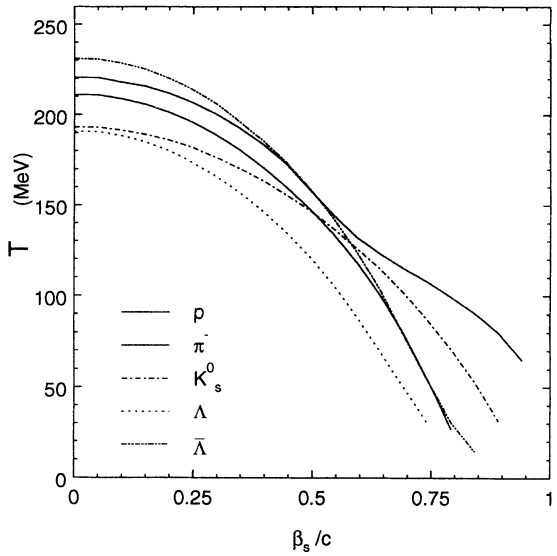

FIG. 2. Every point (T, β_s) on these lines corresponds to a fit of the computed m_T spectra (including resonance decays and transverse flow) to the measured ones [17–19]. Temperature T and transverse flow β_s have similar effects on the spectra so that β_s cannot be extracted unambiguously [15].

produced particles are well described by a boost invariant distribution around the center of the collision zone at $y_{c.m.} = 3$, with the flow rapidities limited to the interval $(-\eta_{max}, +\eta_{max})$ with $\eta_{max} = 1.7 \pm 0.2$ [15] (see Fig. 1).

The situation is less clear for the transverse mass spectra, which are affected both by resonance decays [21] and transverse flow. We found that for any given radial fluid velocity $0 \leq \beta_s \leq 0.7c$ it is always possible to find a temperature $T(\beta_s)$, which fits the spectra for all particle species simultaneously [15] (see Fig. 2). The reason is that with transverse flow the spectra can in good approximation be described in terms of an *apparent* or blueshifted temperature [15]

$$T_{app} = T\sqrt{\frac{1+\langle\beta_r\rangle}{1-\langle\beta_r\rangle}}\,, \tag{1}$$

from which the temperature T and average radial flow $\langle\beta_r\rangle$ cannot be easily separated.

The amount of transverse flow thus cannot be determined from the particle spectra alone. We have shown [22] that the method of global hydrodynamics [16] combined with a realistic freeze-out criterium is well suited to give "circumstantial evidence" for a transverse flow of $\beta_s \approx 0.5\,c$ [23]. Here we will present a more thorough theoretical analysis to gain a better understanding of the dynamics of the collision zone. The method of global hydrodynamics is ideal for such an analysis, because on the one side it contains all necessary elements for a consistent description of the dynamics (coupling of longitudinal and transverse flow by the hydrodynamic equations as well as a dynamical freeze-out criterium) and on the other side, due to its numerical effectiveness, it allows for an in-depth phenomenological analysis including extensive parameter studies.

III. EXTRACTING THE INITIAL CONDITIONS

Hydrodynamics connects the thermalized initial state with the frozen-out final state. With its help the freeze-out conditions (Table I), reflected in the observed particle spectra, can be related to the initial conditions and provide new insights into the dynamical evolution. Some of the initial conditions are known from the size of the projectile nucleus and the measured energy loss of the projectile protons [24,18]. At the freeze-out point we know the maximal fluid rapidity (Fig. 1) as extracted from the y spectra. The $m_\perp$ spectra only yield a correlation between the transverse fluid velocity β_s and the local temperature T at freeze-out (Fig. 2), which is rather difficult to exploit and the discussion of which we postpone until Sec. VI. In principle, it is also possible to determine the final radius using pion interferometry Hanbury-Brown Twiss (HBT) [25]. Unfortunately, up to now the theoretical and experimental uncertainties in the analysis of the two-pion (and two-kaon) correlation functions are still too large (> 0.5 fm) to render them very useful for our purpose [26].

The idea of this paper is to use the global hydrodynamics framework of Ref. [16] to fill in (most of) the question marks in Table I by establishing a connection between the initial and the final states. We proceed strategically and first narrow down the uncertainties in the initial conditions by choosing from all combinations of initial longitudinal flow η_0 and initial energy density ε_0 only those pairs (η_0, ε_0) which after hydrodynamical evolution produce at freeze-out a longitudinal flow value of $\eta_f = 1.7$. In Fig. 3 we show the result for a hadron resonance gas equation of state with specific entropy $S/A = 30$.

For the case of complete stopping (no longitudinal flow at the beginning, $\eta_0 = 0$) we need very high energy densities $\varepsilon_0 > 10\,\mathrm{GeV/fm^3}$, so that the strong longitudinal pressure gradient can accelerate the matter to $\eta_f = 1.7$ at freeze-out. For larger initial flows considerably smaller initial energy densities suffice to reach the same freeze-out value. In the extreme case of very large initial flows $\eta_0 \approx \eta_f$ the system is already close to freeze-out initially; i.e., the initial energy densities are very low, and the hydrodynamics barely generates additional longitudinal flow.

Knowing the possible pairs of initial conditions (ε_0, η_0), we can now study in Fig. 4 the systematics of the hydrodynamically generated transverse flow at freeze-out, parametrized by β_s, within the allowed range of longitudinal flow parameters. Surprisingly, for a large region of initial conditions, ranging from complete stopping to considerable initial transparency ($0 \le \eta_0 \le 1.6$), more or less the same (sizable) amount of transverse flow $\beta_s \approx 0.5c$ is generated [23]. Above $\eta_0 \ge 1.6$ no real hydrodynamical evolution takes place since the matter is already close to freeze-out and is accelerated very little. Although strictly speaking we cannot exclude this possibility within the framework presented here, we will disregard this region from now on, because there the assumption of local equilibrium which underlies the hydrodynamic model breaks

TABLE I. The initial and final state parameters of the global hydrodynamics are only partially known. Through hydrodynamics we can combine our knowledge about the initial and final state and constrain the unknown parameters.

Quantity	Initial state	From	Final state	From
R	4 fm	projectile size	?	(HBT)
β_s	0	defined	(β_s, T)	$\frac{dn}{m_T dm_T}$
Z	from E_{tot}	$E_{\mathrm{loss}} = 313\,\mathrm{GeV}$	?	?
η	?	?	1.7	$\frac{dn}{dy}$
ε	?	?	?	?

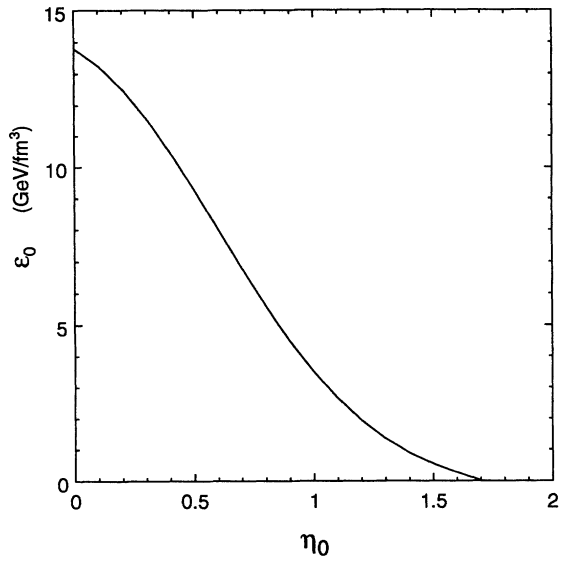

FIG. 3. Shown is the initial energy density $\varepsilon_0(\eta_0)$ which, for a given initial longitudinal flow η_0, generates at freeze-out the measured flow $\eta_f = 1.7$. The hydrodynamics is based on a hadron resonance gas EOS with $S/A = 30$.

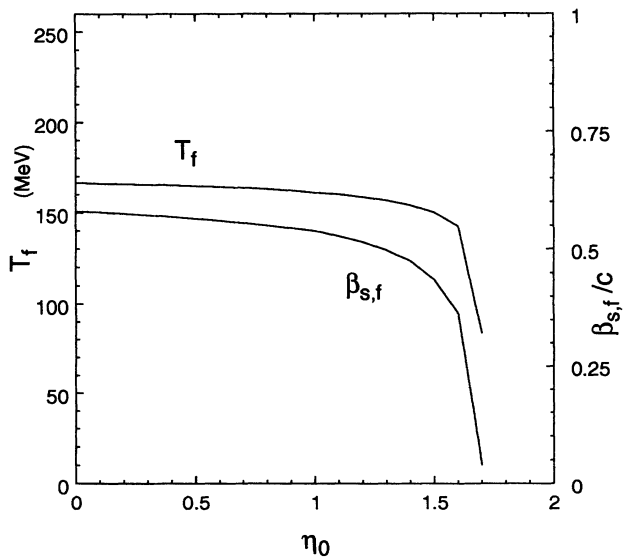

FIG. 4. Temperature T and transverse flow $\beta_{s,f}$ at freeze-out as determined from the longitudinal flow $\eta_f = 1.7$ via the global hydrodynamic model. Both are almost constant over a whole range of initial conditions for the longitudinal flow, $\eta_0 \le 1.6$.

down, and a nonequilibrium description [27] appears to be more suitable.

The temperature at freeze-out turns out to be similarly insensitive to the initial longitudinal flow. This is largely a consequence of the constancy of $\beta_{s,f}$, since the temperature at freeze-out is coupled to the transverse velocity (see Sec. V) via the scattering time scale $\tau_{\rm sca}(T)$ and the expansion time scale $\tau_{\rm exp}(R, Z, \eta_f, \beta_{s,f})$ such that higher velocities cause the system to freeze out already at higher temperatures and densities.

From this we can already conclude that with hadronic observables alone the initial energy density and the initial longitudinal flow cannot be determined. All measurable quantities at freeze-out are essentially independent of η_0 (and thus of ε_0). Other observables, for example, lepton pairs [28], might prove useful to determine the initial energy density: Due to their small cross sections they freeze out immediately and thus the measured spectrum receives contributions from the whole space-time region of the collision zone, with the hot early stages dominating the spectrum due to the T^4 dependence of the Stefan-Boltzmann law for thermal radiation.

IV. FULL STOPPING vs PARTIAL TRANSPARENCY

We will postpone the application of these results for the moment in order to analyze in this section in more detail their dynamical origin. We pick two extreme cases of the initial longitudinal flow which we call, according to their resemblance to the Landau and the Bjorken hydrodynamics, the L scenario ($\eta_0 = 0$) and the B scenario ($\eta_0 = 1.3$), respectively. Their initial and freeze-out values are given in Table II.

The L scenario generates the largest transverse flow, as one would have intuitively expected. But the excess of transverse flow compared to the B scenario is rather small; at first sight this is quite puzzling, considering the large difference in the thermally generated longitudinal flow $\eta_f - \eta_0$, which is 1.7 for the L system and only 0.4 for the B system.

In Fig. 5 we compare the dynamical evolution of both scenarios until freeze-out (where the lines end). The initial time of the B scenario was displaced by hand in such a way that at that point the temperatures in the two scenarios agree. One realizes that the production of longitudinal flow is strongest at the beginning and then levels off considerably, even when taking into account the exponential character of η.

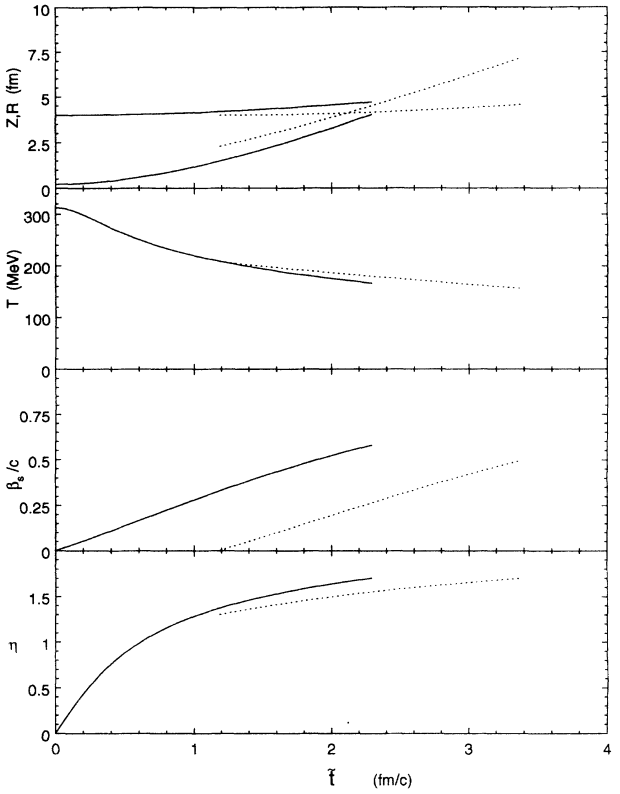

FIG. 5. Comparison between the L scenario (solid lines) and the B scenario (dotted lines) shows remarkable similarities if one shifts the initial time of the B dynamics so that its temperature agrees with the L scenario at some later time. The difference in buildup of transverse flow is compensated by a later freeze-out in the B scenario.

TABLE II. Initial and freeze-out values of the L and the B scenarios, which are distinguished by their initial longitudinal flow η_0, as computed with our model from the known initial values (Table I) and the choice $S/A = 30$ for a hadronic EOS.

		L scenario		B scenario	
		Initial	Final	Initial	Final
R	(fm)	4	4.71	4	4.57
β_s	(c)	0	0.58	0	0.50
Z	(fm)	0.23	4.0	2.3	7.2
η		0	1.7	1.3	1.7
ε	(GeV/fm^3)	13.8	0.36	1.4	0.26
T	(MeV)	313	167	209	157
S/A		30	30	30	30

Neglecting small deviations between both scenarios — which incidentally might also be caused by the slightly differing longitudinally comoving coordinate systems in both cases — the main difference clearly lies in β_s. The L scenario generates transverse flow from the beginning, so that there is already a flow velocity of $\beta_s \approx 0.3c$ when the B system starts. In the further evolution the L system freezes out earlier whereas the B system nearly catches up in transverse flow during the remaining part of its expansion history. The reason for the similar transverse flow velocities at freeze-out thus appears to lie more in the freeze-out criterium than in the initial conditions.

V. LONGITUDINAL AND TRANSVERSE FREEZE-OUT TIME SCALES

We investigate this question in more detail in Fig. 6 by analyzing the dynamically determined expansion time

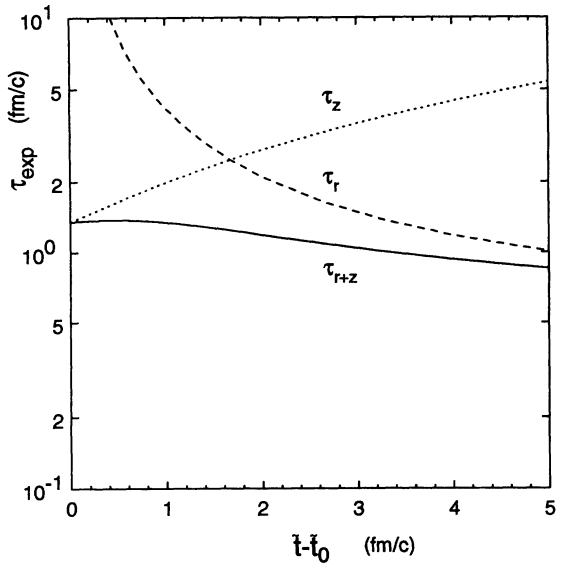

FIG. 6. The expansion time scale (here for the B scenario with $\eta_0 = 1.3$) is initially dominated by longitudinal expansion. After a few fm/c the radial expansion takes over. The net result is a rather weak time dependence of the total expansion time scale.

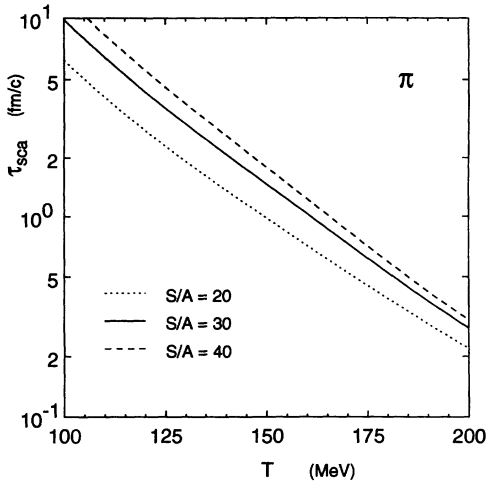

FIG. 7. The scattering time scale of pions in a hadron gas varies with S/A because of the different baryon content. Its exponential decrease at higher temperatures, combined with the near constancy of τ_{exp}, results in freeze-out temperatures which are always close to 150 MeV.

scale τ_{exp}. Initially the evolution is strongly dominated by longitudinal expansion, resulting in small values of τ_{exp}. However, the length of the system quickly increases, reducing the longitudinal velocity gradients and thus weakening the longitudinal shear forces which could break the local thermal equilibrium. A simple estimate in the limit of boost invariant longitudinal expansion gives an expansion time scale $\tau_{exp} = \tilde{t}$ which grows linearly with proper time.

The transverse radius, on the other hand, stays for a long time close to its initial value. Due to quadratic R dependence of the transverse area of the cylinder, already rather small transverse velocities of order $\beta_s \approx 0.4c$ cause appreciable dilution and lead to transverse expansion time scales which can compete with the longitudinal one. This is illustrated by the nonrelativistic estimate [16] $\tau_{exp} \approx (n+1)\beta_s/R \approx 3\,\mathrm{fm}/c$, with $n = 2$ for a quadratic transverse velocity profile and $R = 4\,\mathrm{fm}/c$ for a sulphur nucleus. We conclude that the rarefaction at later stages is strongly dominated by the transverse flow, which thereby limits its own growth. A comparison with the scattering time scale τ_{sca} in Fig. 7, which constitutes our freeze-out criterium $\tau_{exp} = \tau_{sca}$ [29,16], then shows why always nearly the same freeze-out temperature T_f is generated.

Our whole analysis is based on this dynamical freeze-out criterium, which explicitly models the competition between the local expansion, which disturbs equilibrium, and the scattering processes, which restore equilibrium. If we had implemented the freeze-out through a static criterium, e.g., via a freeze-out temperature $T_f = \mathrm{const}$ (typically 140 MeV), this kind of analysis would not have been possible. It is interesting to observe, however, that the result of dynamical freeze-out nearly coincides with such a criterium, due to the rapid cooling of the system by transverse expansion and the exponential temperature dependence of the scattering time scale.

In summary we arrive at the remarkable result that there is no strong correlation between produced longitudinal and produced transverse flow, because the former is mainly generated initially while the latter results from the late dynamical stages before freeze-out. This also explains retrospectively why, in spite of the big differences with regard to the longitudinal dynamics, the spherical model of Ref. [30] yields similar values for the transverse flow at freeze-out.

VI. COMPARISONS WITH THE DATA

We can now confront our theoretical prediction for the relationship between β_s and T at freeze-out with the pairs $(T_f, \beta_{s,f})$ we have extracted from the phenomenology of the transverse mass spectra [15]. The hope is that this comparison permits to narrow down the ambiguity between thermal and collective motion from the phenomenology of the transverse momentum data [15]. However, even though the phenomenological analysis of the data gives an anticorrelation between T_f and $\beta_{s,f}$ according to Eq. (1), whereas the freeze-out criterium correlates T and $\beta_{s,f}$ directly (faster expansion causes freeze-out at higher T), it is *a priori* by no means guaranteed that the two approaches yield comparable (T, β_s) values at all: The only input for the theoretical hydrodynamical model are the rapidity distributions, while its results are checked by using the independent data from the transverse mass distributions.

For the comparison we combine the theoretically determined $\beta_{s,f}(\eta_0)$ and $T_f(\eta_0)$ into a line $(T_f, \beta_{s,f})$, which we parametrize by the unknown initial longitudinal flow η_0, covering the range from 0 to 1.6 as indicated next to the line in Fig. 8. From Fig. 4 we already know that the pairs $(T_f, \beta_{s,f})$ for all initial conditions with genuine hydrodynamical evolution, i.e., for initial flow rapidities $0 \leq \eta_0 \leq 1.6$, are concentrated in a small region near $\beta_s \approx 0.5c$ and $T \approx 150\,\mathrm{MeV}$.

It is gratifying to see in Fig. 8 that the (T, β_s) curve extracted from the data crosses this region; this implies that the phenomenological (T, β_s) correlation is consistent with hydrodynamical evolution and freeze-out, and that our dynamical picture of the collision region successfully explains the data. We can use this agreement between theory and data as support for our assumption of local thermalization and hydrodynamical evolution and interpret the result as a theory-based proof for the existence of transverse flow at freeze-out. To assess the credibility of such an interpretation and to venture into new grounds, we now proceed to examine our analysis under various additional aspects.

The interest for transverse flow in heavy-ion collisions has been fueled also by the hope to find an indicator for a phase transition into the quark-gluon plasma [31]. In an intuitive scenario the initial collision energy in longitudinal direction should be partially converted into the latent heat associated with a first order phase transition. The subsequent cooling and decay of the plasma would then release the energy isotropically to all particles, so that in particular the transverse momenta would profit.

The possible existence of a phase transition to a quark-gluon plasma state influences the hydrodynamical evolution through the corresponding modification of the equation of state (EOS) of the expanding matter. We have tested with the global hydrodynamics quantitatively the equations of state depicted in Fig. 9. They are presented in terms of energy density ε vs pressure P, the variables entering the hydrodynamical tensor $T^{\mu\nu}$. We repeat our procedure to obtain (T, β_s) correlations leaving the unknown initial η_0 open.

We begin by discussing the hadron resonance gas EOS,

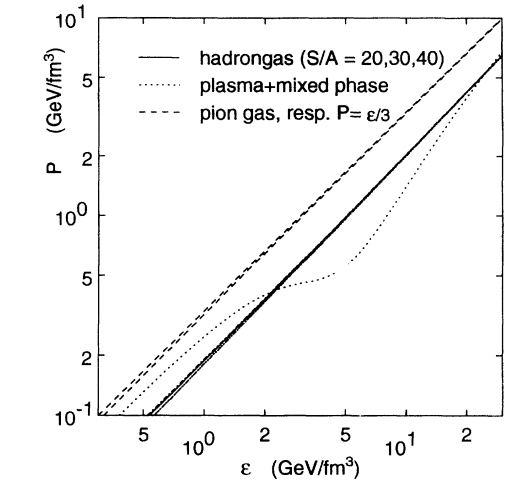

FIG. 9. The equation of state influences the hydrodynamics by the dependence of the pressure $P(\varepsilon)$ on the energy density. There are significant differences between a soft hadron resonance gas (solid line), the plasma equation of state including a phase transition (dotted line), and the hard pure pion gas (dashed line).

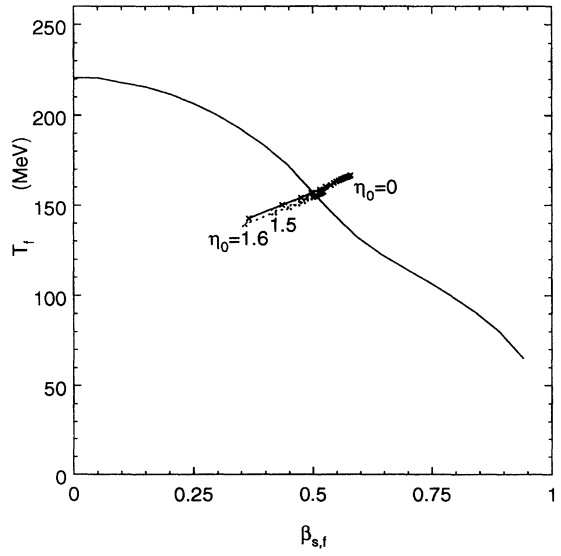

FIG. 8. A comparison of the theoretical correlation between temperature and transverse flow at freeze-out with the experimental correlation deduced from the pion spectra (Fig. 2). The intersection at $\beta_s \approx 0.5c$ can be interpreted as evidence for transverse flow in the experiment. The hydrodynamic system with $\approx 10\%$ entropy generation (dotted line [16]) gives a similar result.

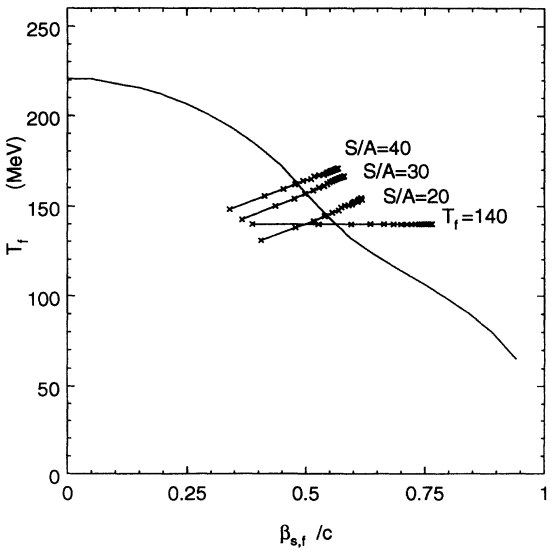

FIG. 10. Sensitivity of the transverse flow to different assumptions: The reference curve from Fig. 8 is labeled by $S/A = 30$. Other hadron resonance equations of state with $S/A = 20$ and 40 result in almost the same transverse flow $\beta_s \approx 0.5c$, whereas freeze-out at constant temperature $T = 140\,\mathrm{MeV}$ leads to a slightly larger transverse flow.

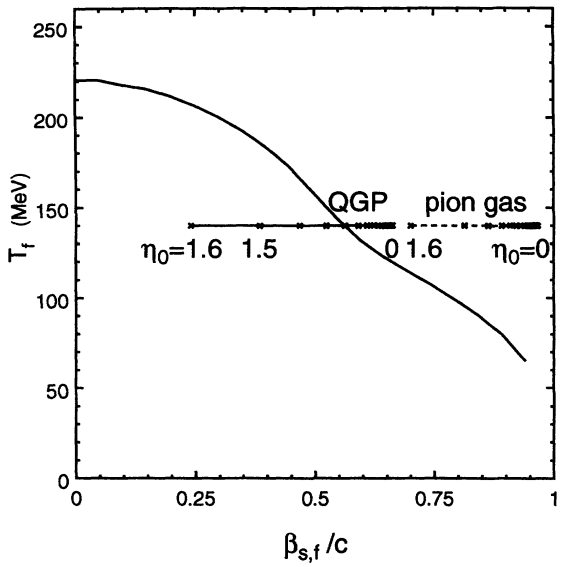

FIG. 11. The transverse flow from a plasma EOS differs only little from that of a hadron resonance gas when the same freeze-out criterium is employed (Fig. 10). For a pure pion gas EOS all initial conditions with genuine hydrodynamical evolution ($\eta_0 \leq 1.5$) generate too much transverse flow and fail to reproduce the data.

which describes a mixture of relativistic ideal gases of a multitude of hadron species (π, η, ρ, ω, ϕ, K^+, K^0, p, n, Δ, Λ, Σ, Ξ, Ω, and their antiparticles). Previously we fixed the entropy per baryon at $S/A = 30$, to achieve agreement with the measured p/π^- ratio (Sec. VII). We now also include the choices $S/A = 20$ and 40, corresponding to systems with larger and smaller baryon densities, respectively. Clearly, all three EOS are very similar in $P(\varepsilon)$ such that the baryon content has little influence on the dynamics. However, due to the large pion-nucleon cross section the baryon content does influence the scattering time scale (Fig. 7). The resulting variations in the freeze-out point can be seen in Fig. 10.

We have also implemented the simple freeze-out criterium $T_f = 140$ MeV = const, as it is often used in hydrodynamics calculations. This also permits us to compare the resonance gas and plasma equations of state, since for the latter the computation of a scattering time scale for the final state hadrons is not really meaningful except near the end of the collision. Because the value of 140 MeV is below the dynamical freeze-out temperatures of our standard scenario, the flow values in this case tend to be somewhat higher.

An extreme, but popular EOS is that of a gas of noninteracting pions. It is much harder [$P_\pi(\varepsilon) \gg P_{\rm had}(\varepsilon)$] than the other equations of state and very close to ideal massless boson limit $P = \frac{1}{3}\varepsilon$. It thus generates a very large transverse flow (Fig. 11), resulting in a known (e.g., [5]) disagreement with the observed m_T spectra. This EOS can thus be excluded by our analysis for all hydrodynamic initial conditions.

Finally we study a plasma equation of state with a first order phase transition, where during the mixed phase plasma and hadron gas coexist. As a representative from this class we have taken the EOS of Ornik *et al.* [32], which has been obtained by interpolation of data points from lattice gauge theory calculations. The plasma EOS exhibits a bend in the coexistence region where the velocity of sound $c_s^2 = \frac{\partial P}{\partial \varepsilon}$ approaches zero. The comparison of Figs. 10 and 11 for $T_f = 140$ MeV shows that the plasma EOS generates a similar amount of flow as the hadron EOS. This results from the fact that the transverse flow is generated at later stages, when the system is no longer in the plasma state but already in the hadron gas phase.

VII. PARTICLE RATIOS AND MULTIPLICITIES

While the thermal description of the momentum spectra follows from the assumption of local thermal equilibrium, which requires only elastic scattering, a thermal description for the relative particle multiplicities (e.g., as in [33]) implies also chemical equilibration which requires additionally inelastic scatterings. While the former seems to be reasonably valid for heavy-ion collisions, the latter is much harder to reach in purely hadronic systems, especially for strange particles [34]. In fact, our approach does yield characteristic discrepancies between theoretical and experimental particle ratios, which indicate that full chemical equilibrium has not been reached in 200 A GeV S+S collisions.

Since particle ratios in a grand canonical description are parametrized by chemical potentials, we now introduce and investigate the dependence on the chemical potentials μ_b for the baryon number and μ_s for the strangeness. While μ_s can be fixed by the condition of local strangeness neutrality ($\rho_s = 0$, corresponding to the initial state of the collision), μ_b at freeze-out can be

TABLE III. The particle ratios from our model in comparison with the data from NA35 [17,19]. The actual number of π^- in the experiment could be smaller than the measured negative hadrons h^- by $\approx 5\%$ because of K^- and $\bar{p}$ contributions, whereas the protons are measured as the difference between positive and negative hadrons.

Experiment			Global hydrodynamics		
	NA35 total y		$S/A = 20$ $T_f \approx 150$ MeV	$S/A = 30$ $T_f \approx 162$ MeV	$S/A = 40$ $T_f \approx 166$ MeV
p/h^-	0.28 ± 0.04	p/π^-	0.45	0.27	0.21
K_s^0/h^-	0.10 ± 0.02	K_s^0/π^-	0.19	0.20	0.21
Λ/h^-	0.080 ± 0.010	Λ/π^-	0.17	0.13	0.11
$\bar{\Lambda}/h^-$	0.015 ± 0.005	$\bar{\Lambda}/\pi^-$	≈ 0.005	≈ 0.015	≈ 0.024

TABLE IV. The total multiplicity and energy of π^- are not very well represented by our model. However, the energy per pion is described rather well. The total entropy per pion is considerably higher than the value of ≈ 4 for a pure pion gas, reflecting the large abundance of heavy particles in the resonance gas. The data are from [18,24].

		Experiment	Global hydrodynamics		
		NA35	$S/A = 20$	$S/A = 30$	$S/A = 40$
N_{π^-}		93 ± 5	55–59	62–67	64–71
E_{π^-}	(GeV)	71 ± 7	45	54	57
E_{π^-}/N_{π^-}	(GeV)	0.76	0.76–0.84	0.81–0.87	0.80–0.89
$S_{\rm tot}/(3N_{\pi^-})$			7.4	6.5	6.2

adjusted by fitting the experimental p/π ratio. We prefer S/A instead of μ_b as a parameter, because it is an invariant of the hydrodynamical evolution and thus can characterize the EOS during the whole expansion.

The particle ratios (including resonance decays) from global hydrodyn mics are shown in Table III in comparison with data from NA35. We compare the total multiplicities, thereby averaging over the rapidity distributions, which may — especially in case of the protons — be different between our model and the experiment (Fig. 5 in [15]). Again the hydrodynamics results are almost independent of the initial longitudinal fluid rapidity η_0. As expected, the p/π^- ratio varies strongly with S/A, and the measured ratio can be reproduced quite nicely by the choice $S/A = 30$. If we would try to account for the reduced baryon content at central rapidities, which is, as mentioned, not fully reproduced by our model for the central zone, we would opt for a value of $S/A = 40$.

The relative multiplicities of the strange particles are generally overestimated by the model, which at first sight seems to indicate that in the experiment chemical equilibrium for strangeness has not been established yet by the $s\bar{s}$ generating processes. In all three cases the value of K_s^0/π^- is almost the same, because the higher kaon abundance at higher temperatures is offset in the denominator by the pion production from increased resonance decay contributions. The $\overline{\Lambda}$ depend very strongly on the freeze-out temperature and the baryon content.

However, the apparent overprediction of the strange particle ratios relative to the negatively charged particles could also be due to an underprediction of the total pion yield by the thermal equilibrium model. As a number of authors have pointed out [35], the pion creation processes might dominate the reverse reaction for some time leading to an overabundance of pions compared to their chemical equilibrium value. Such nonequilibrium features can be modeled by introducing a finite pion chemical potential μ_π. It would attain equal (positive) values for particles and antiparticles, in contrast to the vanishing chemical equilibrium value for bosons without conserved quantum numbers.

Table IV shows that global hydrodynamics is lacking indeed in both the number of pions and their energy. This lack of pion multiplicity accounts for a large fraction of the strange-nonstrange discrepancy between theory and experiment seen in Table III. Therefore the strange sector in S+S collisions is actually much closer to chemical equilibrium than first suspected [36]. This was recently confirmed by a more thorough chemical analysis of the data in [37].

By computing the total energy per pion E_π/N_π, we deduce from the relatively good agreement and the high value of $S_{\rm tot}/N_\pi$ that the discrepancy is not so much a result of the shape of the pion spectrum but merely of the general underrepresentation of the pions in our model relative to strange particles. The observed small deviation in the ratio E_π/N_π could be easily due to the pions in the lowest bin ($m_T - m_\pi \leq 100\,{\rm MeV}/c^2$), which strongly influence the multiplicity because of the exponential character of the m_T spectrum, and which we cannot reproduce in full detail (Figs. 2 and 7 in [15]).

If we were to consider that all the missing pions are generated by strong Bose condensation, we would find (using Boltzmann distributions only) a pion chemical potential of $\mu_\pi = 50 - 80\,{\rm MeV}$ as a rough estimate, without taking into account the effect of a correspondingly harder EOS on the hydrodynamics. This value of μ_π is considerably smaller than $\mu_\pi = 126\,{\rm MeV}$ in [35] and thus sufficiently far away from the Bose divergence at $m_\pi = 139\,{\rm MeV}$ so that it does not lead to a substantial overpopulation at low momenta.

VIII. SUMMARY AND CONCLUSIONS

We started from a previous analysis [15] of hadronic transverse mass and rapidity distributions from 200 A GeV S+S collisions to estimate the maximum information content a hydrodynamic analysis can possibly deliver. Using all available information on both the initial conditions as well as the freeze-out conditions, we still cannot determine the initial longitudinal flow, or equivalently, the initial energy density. However, we find that regardless of the initial flow all possible initial conditions finally lead to the same temperature and transverse flow at freeze-out, which we model with a dynamical freeze-out criterium. This is apparently a consequence of the dynamical freeze-out in conjunction with the transverse expansion, which in the late stages of hydrodynamics proves to be much more important for the rarefaction than the longitudinal expansion.

A comparison with our phenomenological flow analysis shows then good agreement with the data for a wide variety of initial conditions and freeze-out criteria. However, while both hadron resonance gas and plasma equation of

state produce good agreement with the data, a purely pionic equation of state generates too much transverse flow and can thus be excluded for all hydrodynamic initial conditions. Furthermore, from the fact that the data show a lower number of strange particles than our model with chemical equilibrium would produce, we deduce that chemical equilibration has not been reached. On the other hand we determine that the chemical nonequilibrium of pions is not as big as to allow for a μ_π close to the pion mass; we estimate instead $\mu_\pi \approx 50 - 80\,\mathrm{MeV}$.

ACKNOWLEDGMENTS

E.S. gratefully acknowledges support by the Deutsche Forschungsgemeinschaft (DFG), the Alexander-von-Humboldt Stiftung, and the U.S. Department of Energy under Contracts Nos. DE-AC02-76H00016 and DE-FG02-93ER40768. U.H. gratefully acknowledges support by the DFG, the Bundesministerium für Forschung und Technologie (BMFT), and the Gesellschaft für Schwerionenforschung (GSI).

[1] H. Stöcker and W. Greiner, Phys. Rep. **137**, 277 (1986).
[2] H. H. Gutbrod, A. M. Poskanzer, and H. G. Ritter, Rep. Prog. Phys. **52**, 1267 (1989); H. A. Gustaffson *et al.*, Phys. Rev. Lett. **52**, 1590 (1984); R. E. Renfordt *et al.*, *ibid.* **53**, 763 (1984).
[3] H. v. Gersdorff, L. D. McLerran, M. Kataja, and P. V. Ruuskanen, Phys. Rev. D **34**, 794 (1986); M. Kataja, P. V. Ruuskanen, L. D. McLerran, and H. v. Gersdorff, *ibid.* **34**, 2755 (1986).
[4] M. Kataja, Z. Phys. C **38**, 419 (1988).
[5] H. v. Gersdorff, Nucl. Phys. **A525**, 697c (1991).
[6] U. Ornik, F. Pottag, and R. M. Weiner, Phys. Rev. Lett. **63**, 2641 (1989).
[7] R. Waldhauser, D. H. Rischke, U. Katscher, J. A. Maruhn, H. Stöcker, and W. Greiner, Z. Phys. C **54**, 459 (1992); U. Katscher, D. H. Rischke, J. A. Maruhn, W. Greiner, I. N. Mishustin, and L. M. Satarov, Z. Phys. A **346**, 209 (1993).
[8] E. Fermi, Prog. Theor. Phys. **5**, 570 (1950); Phys. Rev. **81**, 683 (1951).
[9] L. D. Landau, Izv. Akad. Nauk SSSR, Ser. Fiz. **17**, 51 (1953) [Bull. Acad. Sci. USSR, Phys. Ser.]; also published in *Collected Papers of L.D. Landau*, edited by D. Ter Haar (Gordon and Breach, New York, 1965).
[10] P. Carruthers and Minh Duong-Van, Phys. Rev. D **8**, 859 (1973).
[11] J. D. Bjorken, Phys. Rev. D **27**, 140 (1983).
[12] Heavy Ion Physics at the AGS, HIPAGS '93, edited by G. S. F. Stephans, S. G. Steadman, and W. L. Kehoe, Massachusetts Institute of Technology Report No. MITLNS-2158, 1993.
[13] "Quark Matter '93," *Proceedings of the 10th International Conference on Ultrarelativistic Nucleus-Nucleus Collisions*, Borlänge, Sweden, 1993, edited by E. Stenlund *et al.* [Nucl. Phys. **A566** (1994)].
[14] NA35 Collaboration, A. Bamberger *et al.*, Phys. Lett. B **184**, 271 (1987); NA35 Collaboration, H. Ströbele *et al.*, Z. Phys. C **38**, 89 (1988); NA34 Collaboration, T. Åkesson *et al.*, *ibid.* **46**, 361 (1990); WA80 Collaboration, R. Albrecht *et al.*, *ibid.* **47**, 367 (1990).
[15] E. Schnedermann, J. Sollfrank, and U. Heinz, Phys. Rev. C **48**, 2462 (1993).
[16] E. Schnedermann and U. Heinz, Phys. Rev. C **47**, 1738 (1993).
[17] NA35 Collaboration, J. Bartke *et al.*, Z. Phys. C **48**, 191 (1990).
[18] S. Wenig, Ph.D. thesis, Universität Frankfurt, 1990, GSI Report No. GSI-90-23, 1990.
[19] NA35 Collaboration., J. Bächler *et al.*, Phys. Rev. Lett. **72**, 1419 (1994).
[20] Yu. M. Sinyukov, V. A. Averchenkov, and B. Lörstadt, Z. Phys. C **49**, 417 (1991).
[21] J. Sollfrank, P. Koch, and U. Heinz, Phys. Lett. B **252**, 256 (1990); Z. Phys. C **52**, 593 (1991); H. W. Barz, G. Bertsch, D. Kusnezov, and H. Schulz, Phys. Lett. B **254**, 332 (1991); G. E. Brown, J. Stachel, and G. M. Welke, *ibid.* **253**, 315 (1991).
[22] E. Schnedermann and U. Heinz, Phys. Rev. Lett. **69**, 2908 (1992).
[23] Please note that we use cylindrical symmetry and a quadratic transverse velocity profile $\beta_r(r,t) = \beta_s(t)[r/R(t)]^2$, such that the average transverse flow velocity $\langle\beta_r\rangle$ is related to the surface expansion velocity β_s by $\langle\beta_r\rangle = 0.5\,\beta_s$. The numerical result thus corresponds to average flow velocities $\langle\beta\rangle = (0.25-0.3)c$ at freeze-out.
[24] NA35 Collaboration, H. Ströbele *et al.*, Nucl. Phys. **A525**, 59c (1991).
[25] G. Goldhaber, S. Goldhaber, W. Lee, and A. Pais, Phys. Rev. **120**, 300 (1960); NA35 Collaboration, A. Bamberger *et al.*, Phys. Lett. B **203**, 320 (1988).
[26] U. Mayer, E. Schnedermann, and U. Heinz, Phys. Lett. B **294**, 69 (1992).
[27] S. Gavin, Nucl. Phys. **B351**, 561 (1991).
[28] M. Kataja, J. Letessier, P. V. Ruuskanen, and A. Tounsi, Z. Phys. C **55**, 153 (1992).
[29] J. Bondorf, S. Garpman, and J. Zimanyi, Nucl. Phys. **A296**, 320 (1978).
[30] K. S. Lee and U. Heinz, Z. Phys. C **43**, 425 (1989); K. S. Lee, U. Heinz, and E. Schnedermann, *ibid.* **48**, 525 (1990).
[31] L. van Hove, Z. Phys. C **27**, 135 (1985).
[32] U. Ornik, F. W. Pottag, and R. M. Weiner, in *Hadronic Matter in Collision 1988*, edited by P. A. Carruthers and J. Rafelski (World Scientific, Singapore, 1989).
[33] *Statistical Mechanics of Quarks and Hadrons*, edited by H. Satz (North-Holland, Amsterdam, 1981).
[34] P. Koch, B. Müller, and J. Rafelski, Phys. Rep. **142**, 167 (1986); H. W. Barz, B.L. Friman, J. Knoll, and H. Schulz, Nucl. Phys. **A484**, 661 (1988).
[35] J. L. Goity and M. Leutwyler, Phys. Lett. B **228**, 517 (1989); M. Kataja and P. V. Ruuskanen, *ibid.* **243**, 181 (1990); S. Gavin, Nucl. Phys. **A544**, 459 (1992).
[36] N. J. Davidson, H. G. Miller, R. M. Quick, and J. Cleymans, Phys. Lett. B **255**, 105 (1991).
[37] J. Sollfrank, M. Gaździcki, U. Heinz, and J. Rafelski, Z. Phys. C **61**, 659 (1994).